

# *Camera-Based Lock-in and Heterodyne Carrierographic Photoluminescence Imaging of Crystalline Silicon Wafers*

**Q. M. Sun, A. Melnikov & A. Mandelis**

**International Journal of  
Thermophysics**

Journal of Thermophysical Properties  
and Thermophysics and Its Applications

ISSN 0195-928X  
Volume 36  
Combined 5-6

Int J Thermophys (2015) 36:1274-1280  
DOI 10.1007/s10765-014-1599-z

Volume 36 • Numbers 5-6 • May-June 2015

## International Journal of Thermophysics

ICPPP-17 Special Issue

IJOT • 10765 • ISSN 0195-928X  
36(5-6) 809-1366 (2015)

 Springer

 Springer

**Your article is protected by copyright and all rights are held exclusively by Springer Science +Business Media New York. This e-offprint is for personal use only and shall not be self-archived in electronic repositories. If you wish to self-archive your article, please use the accepted manuscript version for posting on your own website. You may further deposit the accepted manuscript version in any repository, provided it is only made publicly available 12 months after official publication or later and provided acknowledgement is given to the original source of publication and a link is inserted to the published article on Springer's website. The link must be accompanied by the following text: "The final publication is available at [link.springer.com](http://link.springer.com)".**



# Camera-Based Lock-in and Heterodyne Carrierographic Photoluminescence Imaging of Crystalline Silicon Wafers

Q. M. Sun · A. Melnikov · A. Mandelis

Received: 20 December 2013 / Accepted: 2 April 2014 / Published online: 25 May 2014  
© Springer Science+Business Media New York 2014

**Abstract** Carrierographic (spectrally gated photoluminescence) imaging of a crystalline silicon wafer using an InGaAs camera and two spread super-bandgap illumination laser beams is introduced in both low-frequency lock-in and high-frequency heterodyne modes. Lock-in carrierographic images of the wafer up to 400 Hz modulation frequency are presented. To overcome the frame rate and exposure time limitations of the camera, a heterodyne method is employed for high-frequency carrierographic imaging which results in high-resolution near-subsurface information. The feasibility of the method is guaranteed by the typical superlinearity behavior of photoluminescence, which allows one to construct a slow enough beat frequency component from nonlinear mixing of two high frequencies. Intensity-scan measurements were carried out with a conventional single-element InGaAs detector photocarrier radiometry system, and the nonlinearity exponent of the wafer was found to be around 1.7. Heterodyne images of the wafer up to 4 kHz have been obtained and qualitatively analyzed. With the help of the complementary lock-in and heterodyne modes, camera-based carrierographic imaging in a wide frequency range has been realized for fundamental research and industrial applications toward in-line nondestructive testing of semiconductor materials and devices.

**Keywords** Frequency-domain photoluminescence · Heterodyne carrierography · Lock-in carrierography · Photocarrier radiometry · Silicon wafer

---

Q. M. Sun · A. Mandelis  
School of Optoelectronic Information, University of Electronic Science and Technology of China,  
Chengdu 610054, China

Q. M. Sun · A. Melnikov · A. Mandelis (✉)  
Center for Advanced Diffusion-Wave Technologies (CADIFT), Department of Mechanical  
and Industrial Engineering, University of Toronto, Toronto, ON M5S 3G8, Canada  
e-mail: mandelis@mie.utoronto.ca

## 1 Introduction

Lock-in thermography (LIT) and steady-state and dynamic photoluminescence (PL) have been demonstrated to be powerful imaging techniques for nondestructive, non-contact, and all-optical semiconductor diagnostics [1–8]. Laser-induced photocarrier radiometry (PCR), a form of dynamic modulated PL, was introduced by Mandelis et al. [9]. PCR has proven to be an effective quantitative methodology for carrier transport parameter determination and carrier density imaging of Si wafers and solar cells [10–12].

Recently, camera-based lock-in carrierography (LIC), which uses two spread illumination laser beams and a near-infrared (NIR) InGaAs camera, has been introduced as an imaging extension of single-element InGaAs detector PCR [11, 13, 14]. LIC is a self-calibrating and quantitative imaging methodology which eliminates the requirement for calibration in conventional PL imaging [15, 16]. However, only at high frequencies ( $\omega\tau \gg 1$ , where  $\omega$  is the modulation angular frequency and  $\tau$  is the effective carrier lifetime), can LIC images of Si-based devices yield much improved and needed spatial (both radial and axial) resolution of optoelectronic defects at shallow depths below the illuminated surface [14]. This high-frequency requirement poses a severe technical challenge to the speed of today's NIR cameras.

High-frequency camera imaging was first achieved by Grauby et al. [17] in the photothermal field, using a heterodyne scheme. The key to the heterodyne method is to construct a slow enough beat frequency component through nonlinear frequency mixing. There are mainly two different sources of nonlinearity involved in heterodyne imaging techniques: one is the detector with nonlinear response [17, 18]; another is the sample itself [14]. Because of the typical superlinearity behavior of PL [19], Si-based devices can act as a natural frequency mixer for high-frequency heterodyne carrierographic (HDC) imaging. In this paper, LIC images up to 400 Hz of a crystalline Si wafer with a mechanically damaged back-side small area are presented. PCR intensity-scan measurements of the wafer were carried out, and the nonlinearity of the wafer was experimentally verified. HDC images up to 4 kHz have been obtained and qualitatively analyzed.

## 2 Experimental

A schematic of the carrierography experimental setup was shown in [14]. The sample under investigation was a p-type high-quality crystalline silicon wafer with a thickness of 690  $\mu\text{m}$ . A small area on the back surface of the wafer was mechanically damaged through gentle rubbing with a piece of fine sandpaper. Optical illumination was performed by two fiber-coupled 9 W, 808 nm diode lasers. The laser beams were spread and homogenized by microlens arrays forming a  $10 \times 10 \text{ cm}^2$  square illumination area with intensity variations  $<5\%$  across that area. A high-speed NIR InGaAs camera (Goodrich SU320KTSW-1.7RT/RS170) was used with  $320 \times 256$  pixel active elements, spectral bandwidth of 0.9  $\mu\text{m}$  to 1.7  $\mu\text{m}$ , frame rate of 120 fps for full window size, and exposure times of 0.13 ms to 16.6 ms. A long-pass filter (Spectrogon LP-1000 nm) was used in front of the camera to filter out the excitation laser. Syn-

chronous undersampling with the external trigger of the camera was implemented by a data acquisition module (NI USB-6259) to overcome the frame rate limitation. Sixteen images per correlation period were recorded by the computer with a frame grabber (NI PCI-1427) to produce high-SNR in-phase/quadrature and amplitude/phase images. All measurements were carried out at room temperature in the dark.

For LIC, the data acquisition module was used to generate a square waveform for laser current modulation, to trigger frame acquisition signals in the camera, and to provide a reference from one of its analog outputs. Both lasers were modulated simultaneously in-phase and at the same frequency. The exposure time was chosen to be 0.52 ms, so it could follow a modulation frequency up to 400 Hz. For HDC, the two lasers were sinusoidally modulated by a two-channel function generator (Agilent Technology 81150A-002) with a 10 Hz frequency difference. The 10 Hz reference and the trigger were produced by the data acquisition module. For synchronization of all signals, the modulation was started at the first sampling instant and was stopped at the end of each correlation period. The exposure time was chosen to be 2.08 ms for a compromise between SNR and camera saturation.

For intensity-scan measurements, the conventional single-detector PCR system was employed [7]. A 30 mW, 830 nm diode laser with a beam diameter of approximately 0.1 mm was square-wave modulated. A density-variable rotational neutral filter (Thorlabs NDC-100C-2M) was used to continuously change the excitation intensity. One percent of the total laser energy was split off for intensity monitoring. A long-pass filter was placed in front of the InGaAs detector (Thorlabs PDA400) to block the excitation beam. Thermal-infrared photon contributions to the signal were eliminated by the long-wavelength cut-off of the InGaAs detector. Two lock-in amplifiers measured the amplitudes of the excitation intensity and PCR signal, respectively.

### 3 Results and Discussion

LIC images of the wafer at 400 Hz are shown in Fig. 1. There is substantial contrast in both amplitude and phase images with the damaged area located at the bottom center. The physical origin of the contrast in the images is related to variations in modulated carrier density. A qualitative comparison between amplitude and phase images shows the expected correspondence: the large amplitude is due to high carrier density, i.e., long local effective carrier recombination lifetime and thus large phase lag. The mechanical damage on the back side has led to a significant reduction in the effective carrier recombination lifetime and an increase in the back surface recombination velocity (SRV). Accordingly, both amplitude and phase lag in the damaged area are smaller. For quantitative purposes, only the phase image was used due to its absolute nature and independence of surface reflectance variations. A simplified model was used to calculate the local effective carrier lifetime from the phase lag image [3] at 400 Hz [15]:

$$\tau_e = -\tan \varphi / \omega. \quad (1)$$

Here  $\tau_e = (\tau_b^{-1} + \tau_s^{-1})^{-1}$ , where  $\tau_b$  is the bulk lifetime and  $\tau_s$  is the surface lifetime, a function of the SRVs and the sample dimensions. Due to low-frequency response

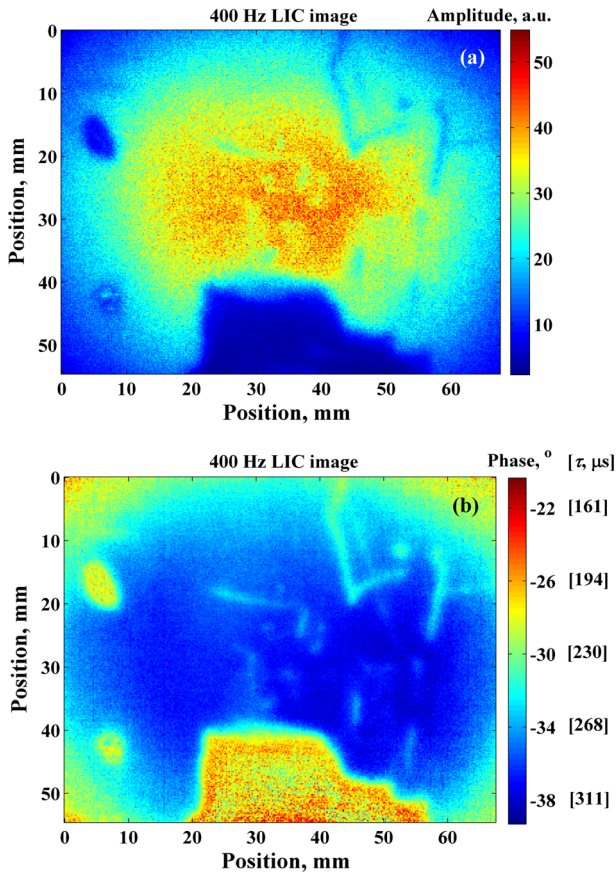


**Fig. 1** 400 Hz LIC images of a Si wafer with mechanical back-side damage: (a) amplitude and (b) phase and carrier effective lifetime

limits of cameras associated with LIC, it is impossible to evaluate the bulk lifetime and SRVs. According to the phase lag distribution shown in Fig. 1b, using Eq. 1, it is found that the effective lifetime of the wafer ranges from approximately  $160 \mu\text{s}$  to  $320 \mu\text{s}$ , also shown in Fig. 1b. The small features around the center are caused, probably, by some defect blotches on the sample surfaces. A comparison between amplitude and phase images shows the features are less obvious in the phase image because the phase signal is independent of the variable reflectance on the sample surfaces. It should be mentioned that the influence of the nonlinearity on the PCR phase at low frequency, according to our simulation, is negligible. Therefore, for the quantitative analysis of low-frequency LIC images, it is not necessary to take the nonlinearity into account.

Free carrier recombination can be classified as two kinds: one-body processes (carrier-to-dopant and carrier-to-defect) and two-body processes (carrier-to-carrier). Physically,  $\gamma$  is determined by which kind of process dominates, and is often related to the doping concentration, the injection level, the defect-state density, etc. Usually,  $\gamma$  is between 1 and 2 [19]. Figure 2 shows the dependence of the PCR amplitude on

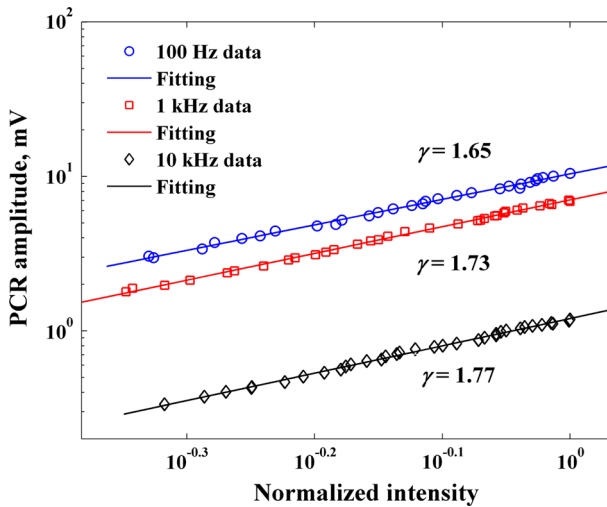


**Fig. 2** PCR intensity scans at the central part of the wafer at 100Hz, 1kHz, and 10kHz

the excitation intensity at 0.1 kHz, 1 kHz, and 10 kHz. The wafer location chosen for the intensity-scan measurement is in the central intact area. From the fitting results, one can see the nonlinearity exponent  $\gamma$  (defined by  $A = I^\gamma$ ,  $A$  is the amplitude and  $I$  is the excitation intensity) is around 1.7 for intact regions in the abovementioned frequency range. It should be mentioned that the experimentally determined nonlinear coefficient in the damaged region is somewhat larger, but close to 1.7. The similarity between the two exponents shows that the impact of back surface damage on the bulk properties is not significant. These experimental results provide a solid basis for high-frequency HDC imaging of the wafer.

Figure 3 shows two HDC amplitude images of the wafer at 600 Hz and 4 kHz. It can be seen from Fig. 3a that the 600 Hz HDC image is similar to the LIC images in Fig. 1, except for some visible small features in Fig. 1 which disappear in Fig. 3a. However, the damaged area located at the bottom center of the image is still clearly seen. For the 4 kHz HDC image, shown in Fig. 3b, the  $\omega\tau > 1$  condition is now satisfied, and the ac diffusion length becomes shorter. In this case, the influence of the wafer back surface on the image is weakened, and one can see that the contrast decreases in most of the imaged area and the image becomes much more homogenous than those at the lower frequencies. However, the damaged area now exhibits a larger heterodyne amplitude than the intact area, which means HDC reverses and highlights image contrast from defective regions against a fading background in high-quality wafer regions. Contrast reversal was observed due to the fact that for low-frequency images, the signal amplitude scales with lifetime  $\tau$ : the longer the lifetime, the higher is the amplitude. Therefore, electronically intact regions exhibit high signal and defective regions show contrast due to the associated shorter lifetime and lower signal. However, when high-frequency heterodyne imaging at, or above,  $f_1 \sim 1/2\pi\tau_{\text{intact}}$  is attained, then the amplitude of the intact region tends to dive steeply because the carrier recombination rapidly goes out of phase with the modulated laser illumination. When it crosses over

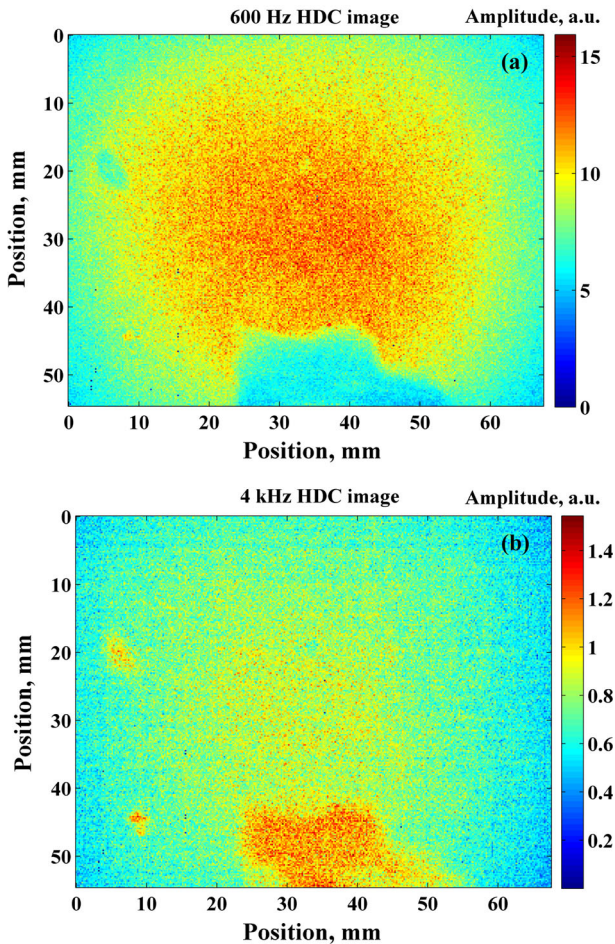


**Fig. 3** HDC amplitude images of the wafer at (a) 600Hz and (b) 4kHz; the same area as in Fig. 1

the amplitude of the defective region, then regions that used to exhibit high amplitudes at low frequencies now exhibit low amplitudes, and defective regions exhibit higher amplitudes as the out-of-phase condition,  $f_2 \sim 1/2\pi\tau_{\text{defect}}$  is not yet met. This is the source of contrast inversion, and modulation at  $f > f_2$  highlights the presence of defect regions over a low intact signal background.

#### 4 Conclusions

LIC and HDC imaging of a crystalline Si wafer were introduced. Quantitative LIC amplitude and phase images of the wafer up to 400 Hz were presented. HDC has allowed the realization of high-frequency ( $\omega\tau > 1$ ) optoelectronic imaging; the signal is closely related to the PCR nonlinearity as well as the transport parameters of the

sample. HDC allows for shallow device subsurface regions such as junctions to be imaged closer to the surface, which is an excellent tool for optoelectronic quality assurance and wafer fabrication control throughout all phases of device processing.

**Acknowledgments** The authors are grateful to NSERC for a Discovery grant, to the Canada Foundation for Innovation for equipment grants, and to the Ontario Ministry for Research and Innovation for the Inaugural Premier's Discovery Award in Science and Technology (2007). QMS gratefully acknowledges the Academic Support Program for Outstanding PhD of UESTC, and the Central-University Basic Research Fund of UESTC (Grant No. ZYGX2012Z006).

## References

1. P. Pohl, J. Schmidt, C. Schmiga, R. Brendel, J. Appl. Phys. **101**, 073701 (2007)
2. M. Kasemann, M.C. Schubert, M. The, M. Köber, M. Hermle, W. Warta, Appl. Phys. Lett. **89**, 224102 (2006)
3. K. Ramspeck, K. Bothe, J. Schmidt, R. Brendel, J. Appl. Phys. **106**, 114506 (2009)
4. T. Trupke, R.A. Bardos, M.C. Schubert, W. Warta, Appl. Phys. Lett. **89**, 044107 (2006)
5. I. Riisness, C. Carach, M.J. Gordon, Appl. Phys. Lett. **100**, 073308 (2012)
6. A. Delamarre, L. Lombez, J.F. Guillemoles, Appl. Phys. Lett. **100**, 131108 (2012)
7. S. Herlufsen, K. Bothe, J. Schmidt, R. Brendel, S. Siemund, Sol. Energy Mater. Sol. Cells **106**, 42 (2012)
8. D. Kiliani, G. Micard, B. Steuer, B. Raabe, A. Herguth, G. Hahn, J. Appl. Phys. **110**, 054508 (2011)
9. A. Mandelis, J. Batista, D. Shaughnessy, Phys. Rev. B **67**, 205208 (2003)
10. J. Batista, A. Mandelis, D. Shaughnessy, B. Li, Appl. Phys. Lett. **85**, 1713 (2004)
11. A. Melnikov, A. Mandelis, J. Tolev, P. Chen, S. Huq, J. Appl. Phys. **107**, 114513 (2010)
12. A. Melnikov, B. Halliop, A. Mandelis, N.P. Kherani, Thin Solid Films **520**, 5309 (2012)
13. A. Mandelis, Y. Zhang, A. Melnikov, J. Appl. Phys. **112**, 054505 (2012)
14. A. Melnikov, P. Chen, Y. Zhang, A. Mandelis, Int. J. Thermophys. **33**, 2095 (2012)
15. Q. Sun, A. Melnikov, A. Mandelis, Appl. Phys. Lett. **101**, 242107 (2012)
16. J. Liu, A. Melnikov, A. Mandelis, J. Appl. Phys. **114**, 104509 (2013)
17. S. Grauby, B.C. Forget, S. Hole, D. Fournier, Rev. Sci. Instrum. **70**, 3603 (1999)
18. E. Absil, G. Tessier, M. Gross, M. Atlan, N. Warnasooriya, S. Suck, M. Coppey-Moisan, D. Fournier, Optics Express **18**, 780 (2010)
19. T. Schmidt, K. Lischka, Phys. Rev. B **45**, 8989 (1992)